

Symmetry of surface states

E. Bertel

Max-Planck-Institut für Plasmaphysik, EURATOM-Association, D-85740 Garching, Germany

(Received 19 April 1994)

The symmetry of surface states on metal surfaces is investigated by group-theoretical methods. The surface states are represented in the linear-combination-of-atomic-orbitals approximation. This approach yields a qualitative characterization of surface states with respect to their orbital composition, charge distribution, position of nodal planes, etc., simply on the basis of existing bulk-band-structure calculations. Symmetry selection rules are easily derived and examples are given, where erroneous assignments and ambiguities in the literature could be clarified by the present method.

Surface states (SS's) on metal surfaces, traditionally being considered as volatile entities with little physical significance, nowadays are subject to a surging interest in surface physics.¹ For instance, SS's can induce reconstructions via Peierls transitions,² give rise to a nonadiabatic damping of adsorbate vibrations,³ and determine the range of adsorbate-adsorbate interactions.^{4,5} The scattering of SS's on defects was directly imaged in scanning tunneling microscopy.⁶ Second-harmonic-generation (SHG) experiments confirmed the contribution of SS's to the nonlinear optical response of metal surfaces.⁷ Last, but not least, SS's have been shown to play a crucial role in surface and thin-film magnetism.⁸⁻¹²

Given the wide range of phenomena where SS's are involved, it is desirable to develop a thorough understanding of SS properties. Recent reviews provide an excellent insight into the basic theory of SS's.^{13,14} The present paper aims in particular at exploring the symmetry properties of SS's. As SS's are two-dimensional eigenstates of the surface Hamiltonian H_S , they can be expanded into basis functions belonging to the irreducible representations of the symmetry group G_S of H_S . These basis functions can be generated by projection-operator techniques.¹⁵ It is particularly illuminating to use a linear combination of atomic orbitals (LCAO) as the starting point for such a procedure. In this way, one obtains symmetry-adapted SS wave functions, which are very convenient for visualizing SS wave functions, analyzing their symmetry, and interpreting experimental results.

In order to obtain a LCAO representation of SS's, we elaborate somewhat upon an idea that was originally proposed by Louie *et al.*:¹⁶ Inside the crystal a SS $\Psi_{\mathbf{k}_\parallel}(\mathbf{r})$ may be expanded into bulk Bloch states $\Phi_{n,\mathbf{k}}(\mathbf{r})$ to the same \mathbf{k}_\parallel as follows: $\Psi_{\mathbf{k}_\parallel}(\mathbf{r}) = \sum_{n,\mathbf{k}_\perp} a_{n,\mathbf{k}_\perp} \Phi_{n,(\mathbf{k}_\parallel,\mathbf{k}_\perp)}(\mathbf{r})$. Real energy eigenvalues in a gap, as they are required for the existence of stationary states, can only be obtained if \mathbf{k}_\perp is allowed to take complex values $\mathbf{k}_\perp = \boldsymbol{\kappa} + i\boldsymbol{\mu}$. The imaginary part of \mathbf{k}_\perp determines the decay length of the SS's into the bulk.^{17,18} By use of the LCAO approximation for the bulk states $\Phi_{n,\mathbf{k}}$, one obtains an expansion of the SS's in terms of atomic orbitals $\chi_l(\mathbf{r} - \mathbf{R}_j)$ centered at the lattice sites \mathbf{R}_j

$$\Psi_{\mathbf{k}_\parallel}(\mathbf{r}) = \sum_j e^{i\mathbf{k}_\parallel \cdot \mathbf{R}_j} \sum_{\mathbf{k}_\perp} e^{i\boldsymbol{\kappa} \cdot \mathbf{R}_j} \sum_n \tilde{a}_{n,\mathbf{k}_\perp}(z) \sum_l b_{nl} \chi_l(\mathbf{r} - \mathbf{R}_j). \quad (1)$$

Here, $\tilde{a}_{n,\mathbf{k}_\perp}(z) = e^{\mu z} a_{n,\mathbf{k}_\perp}$. The term $\sum_l b_{nl} \chi_l(\mathbf{r} - \mathbf{R}_j)$ gives the atomic-orbital composition of band n . For the sake of concreteness, let us examine the Cu(111) surface. The corresponding bulk and surface Brillouin zone (SBZ) is shown in Fig. 1(a). At the center of the SBZ there are SS's that are associated with the large band gap between the $L_{2'}$ and the L_1 point of the bulk band structure. The atomic-orbital composition of the $L_{2'}$ band is $(x + y + z)/\sqrt{3}$ (Ref. 15, pp. 128-136). This is an atomic $p_{z'}$ state, where z' is a coordinate along the ΓL direction (i.e., along the surface normal). L_1 contains 1 (s state) and $1/2\sqrt{3}\{3[(x + y + z)/\sqrt{3}]^2 - r^2\}$ ($d_{z',2}$ state). Thus, the L_1 state can be written as $\sum_l b_{L_1 l} \chi_l(\mathbf{r} - \mathbf{R}_j) = b_s s + b_d d_{z',2}$, which are $sd_{z',2}$ hybrid functions (the exact value of b_s and b_d can only be determined from a full-blown band-structure calculation).

The coefficients $\tilde{a}_{n,\mathbf{k}_\perp}(z)$ contain an exponential damping of the SS's towards the interior of the crystal.^{17,18} They also determine the relative contribution of different bands to the SS wave function. For instance, the SS in the vicinity of E_F at the Γ point of the Cu(111) surface^{18,19} is located close to the $L_{2'}$ point. Consequently, it has predominantly $p_{z'}$ character and $\tilde{a}_{L_{2'},\mathbf{k}_\perp}$ is much larger than $\tilde{a}_{L_1,\mathbf{k}_\perp}$.

Finally, the first two factors of expansion (1) give the phase shift parallel (perpendicular) to the surface from atom to atom or layer to layer, respectively. In our example, $\mathbf{k}_\parallel = 0$ at the Γ point and, therefore, the SS at E_F consists essentially of a bonding combination of $p_{z'}$ orbitals. Accordingly, an upward dispersion is expected for finite \mathbf{k}_\parallel in agreement with experiment.¹⁹ The resulting SS [Fig. 1(b)] is a plane wave with wave fronts parallel to the surface and nodal planes coinciding with the atom layers. This result agrees perfectly with the representation of the SS's obtained from the nearly-free-electron theory.²⁰

In order to analyze their symmetry properties, we expand the SS's into basis functions for the irreducible representations of the symmetry group G_S of H_S (see Chap. 3, Sec. 6 of Ref. 15). For this purpose, we apply the appropriate projection operators to the LCAO representation. The expansion of a SS into the basis functions of a particular irreducible representation $\mathfrak{R}_{\mathbf{k}_{\parallel}m}$ of G_S includes only two-dimensional Bloch functions, which have the same wave vector \mathbf{k}_{\parallel} and are basic functions for the irreducible representation \mathfrak{R}_m of the (point) group of \mathbf{k}_{\parallel} (see Chap. 5, Sec. 2.2 of Ref. 15). This yields the following recipe for the construction of symmetry-adapted SS wave functions. (i) From the energy E and the parallel wave vector \mathbf{k}_{\parallel} of the SS's under consideration, the corresponding gap in the bulk band structure is determined. (ii) From the bulk band structure, a representation of the SS is obtained in the form of an expansion (1) into LCAO bulk states. (iii) The group of \mathbf{k}_{\parallel} is determined and the

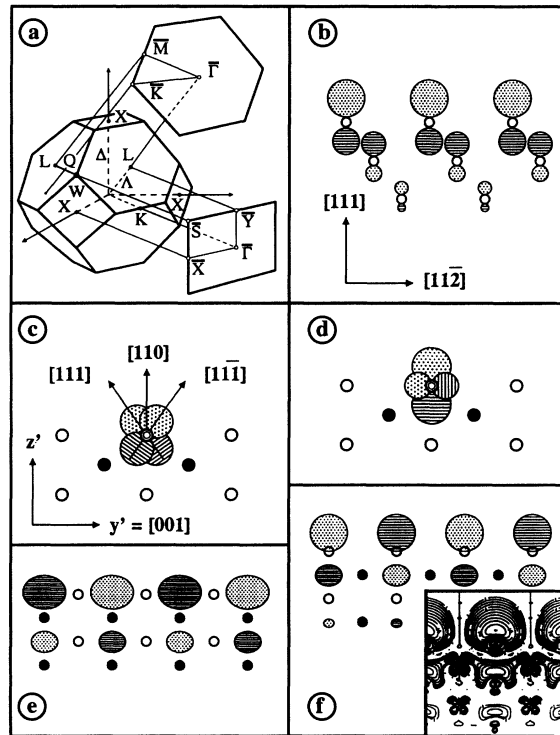


FIG. 1. (a) The fcc bulk Brillouin zone and the surface Brillouin zones for the (111) and the (110) surfaces. (b) Schematic LCAO representation of the $\bar{\Gamma}_1$ surface state on Cu(111). The open circles indicate atom positions in the three topmost Cu layers, the shaded circles represent the $p_{z'}$ -type orbitals. A different sign of the wave function is indicated by different shading. (c) $p_{(111)}$ orbitals of a surface atom on Cu(111). The open and closed circles represent atoms in and below the cross-section plane, respectively. (d) Symmetrized linear combinations of the $p_{(111)}$ orbitals shown in (c). (e) Schematic LCAO representation of the $p_{y'}$ (\bar{Y}_4) surface state at \bar{Y} on Cu(110). (f) Schematic LCAO representation of the $p_{z'}$ (\bar{Y}_1) surface state at \bar{Y} on Cu(110). Inset: Charge-density distribution of the Cu(110) $p_{z'}$ surface state after Ref. 27. Here, the cut is oriented in the $[11\bar{2}]$ azimuth.

projection operators P_m for the various irreducible representations \mathfrak{R}_m are constructed.²¹ (iv) The projection operators are applied to the SS representation constructed in (ii). The result is either a symmetry-adapted SS wave function or zero, if the bulk states are orthogonal to the basis functions of that particular irreducible representation. In the following, we use this recipe to discuss some of the SS's occurring at the low-index fcc surfaces of transition metals.

The Cu(111) example is a nearly trivial case. The group of $\mathbf{k}_{\bar{\Gamma}}$ is C_{3v} . The $p_{z'}$ SS transforms into itself under all symmetry operations of C_{3v} . Accordingly, the projection operator P_1 for the totally symmetric representation reproduces the SS wave function, whereas all other projection operators of C_{3v} yield zero. The same statement applies for the $sd_{z,2}$ hybrid function representing the L_1 state. Thus, at $\bar{\Gamma}$ we find only totally symmetric $\bar{\Gamma}_1$ (Ref. 22) SS's in the $L_2 - L_1$ gap. The d states from the L_3 point, which lies close to the L_2 point, cannot mix into the $\bar{\Gamma}_1$ SS, because application of the projection operator P_1 to the LCAO representations of L_3 yields zero.

Next, we investigate the SS in the \bar{Y} gap of a Cu(110) surface, where two SS's have been observed by photoemission²³⁻²⁵ and inverse photoemission,^{25,26} respectively. As in the previous example, the gap opens between the L_2 and the L_1 point of the bulk band structure. The L_2 LCAO representation $(x+y+z)/\sqrt{3}$ corresponds to a p orbital in the $[111]$ direction [Fig. 1(c)]. The group of $\mathbf{k}_{\bar{Y}}$ is C_{2v} and possesses four one-dimensional irreducible representations. When applying the projection operators P_m to expansion (1), we remember that $P_m \sum_j e^{i\mathbf{k}_{\parallel} \cdot \mathbf{R}_j} \chi_l(\mathbf{r} - \mathbf{R}_j) = \sum_j e^{i\mathbf{k}_{\parallel} \cdot \mathbf{R}_j} P_m \chi_l(\mathbf{r}_j)$, where \mathbf{r}_j is replaced by $(\mathbf{r} - \mathbf{R}_j)$ after P_m has been applied (see Ref. 15, p. 144). Therefore, it is sufficient to consider the effect of the projection operators on the atomic orbitals. For an atom at a position \mathbf{R}_j , where $\mathbf{k}_{\parallel} \cdot \mathbf{R}_j = n\pi$, P_1 yields a symmetric linear combination $p_{[111]} + p_{[11\bar{1}]}$, whereas P_4 yields the antisymmetric combination $p_{[111]} - p_{[11\bar{1}]}$. The other projection operators yield zero. With $z' = [110]$ (surface normal), $y' = [001]$, and $x' = [1\bar{1}0]$ as usual²⁵ the symmetric combination corresponds to a $p_{z'}$ -type orbital and the antisymmetric combination to a $p_{y'}$ orbital. This is shown in Fig. 1(d). For an atom at a position \mathbf{R}_j , where $\mathbf{k}_{\parallel} \cdot \mathbf{R}_j = (2n+1)\pi/2$, application of P_1 yields a $p_{y'}$ and of P_4 a $p_{z'}$ orbital.

The wave functions for the \bar{Y}_1 and the \bar{Y}_4 SS's can now be obtained by coupling the symmetrized atomic orbitals according to expression (1). The result is shown schematically in Figs. 1(e) and 1(f). There is no phase change in the x' direction (i.e., perpendicular to the drawing plane), because at \bar{Y} , $k_{x'} = 0$. Thus, both states are bonding along the rows. Across the rows, the $p_{y'}$ state is a σ bonding state, whereas the $p_{z'}$ state is π antibonding²⁵ (the origin has been chosen to lie in a surface atom). The probability distribution of the $p_{y'}$ state peaks within the surface. In contrast, the $p_{z'}$ state resembles a typical dangling-bond state. For these reasons, the $p_{y'}$ state is lower in energy and differs from the bulk L_2 state by only a small

amount of energy. The dangling-bond p_z state, being strongly disturbed by the absence of the next layer, is driven towards the middle of the gap. Therefore, one needs to take into account the contribution from the upper gap edge (L_1), which is non-negligible for a state in the middle of the gap. Application of the projection operators to an s wave yields only a \bar{Y}_1 contribution. Application of P_1 to the d contribution in $L_1(xy + yz + xz)$ yields xy , which translates to $z'^2 - x'^2$ in our surface coordinates. $P_4(xy + yz + xz)$ yields $z(x + y)$, which corresponds to $z'y'$. Thus, the p_z SS may hybridize with s and $d_{z^2-x^2}$ atomic orbitals. The p_y SS at the lower gap edge could mix with $d_{z'y'}$. The d admixture, however, will be very small, because the SS is nearly degenerate with the purely p -derived bulk L_2 state. A comparison of the p_z SS wave function obtained in this way with a first-principles calculation of the corresponding unoccupied SS on Cu(110) (Ref. 27) is shown in Fig. 1(e). The most important qualitative difference is the neglect of the d contribution in our schematic wave function. As the d contribution is rather localized, it will have only a minor effect on surface properties such as nonlinear polarizability, tunneling current, etc. The contribution of the SS to chemical bond formation will, in general, also be dominated by the sp component. Therefore, the more relevant features of the SS wave function are very well represented by the simple schematic picture shown in Fig. 1.

On Ag(110), analogous SS's are obtained.^{28,29} Urbach *et al.*⁷ demonstrated that these SS's yield a strong resonance in the SHG signal. This is plausible from Figs. 1(d) and 1(e), which show that an excitation from the partially occupied p_y to the partially unoccupied p_z SS is associated with a considerable shift of the charge centroid. The corresponding selection rules are easily derived: The z' (y', x') components of the dipole operator transform as the \bar{Y}_1 (\bar{Y}_4, \bar{Y}_3) irreducible representations. Accordingly, the $p_y \rightarrow p_z$ transition is excited only by y' -polarized radiation, as it was indeed observed experimentally.⁷

A further interesting problem amenable to investigation by the present method is the SS's at the \bar{S} point of the Ni(110) surface. The temperature dependence of the SS exchange splitting at the \bar{S} point was used by Eberhardt *et al.*⁸ to test various models for the temperature dependence of surface magnetism. The bulk bands, which are relevant for the \bar{S} point, extend along the Q line [Fig. 1(a)] and are shown for Ni in Fig. 2. The group of \mathbf{k}_\parallel at \bar{S} is C_{2v} . Eberhardt *et al.*⁸ assigned the two SS features appearing close to E_F in their ultraviolet photoemission spectra to a pair of exchange split SS's in a Q_2 band gap. Kleinman³⁰ pointed out that a Q_2 band gap can support only \bar{S}_3 and \bar{S}_4 SS's, which, however, were not found in his calculations. According to Kleinman's assignment,³⁰ the exchange-split features observed by Eberhardt *et al.*⁸ could only be attributed to a pair of \bar{S}_2 SS's in a Q_1 band gap.

After having reexamined the case by the projection-operator technique, we find in agreement with Kleinman³⁰ that the \bar{S}_1 and \bar{S}_2 SS's occur in the Q_1 band gaps, whereas the Q_2 band gaps support only \bar{S}_3 and \bar{S}_4 SS's.

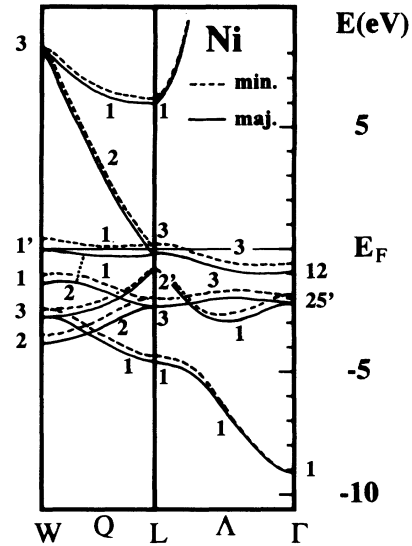


FIG. 2. Section of the Ni bulk band structure. The topology of the bands follows essentially the calculations of Eckardt and Fritsche (Ref. 34). The L_2 point and the L_3 points were adjusted to the experimental values given by Himpsel and Eastman (Ref. 31).

The highest d -band gap of Q_1 symmetry (Fig. 2, dotted line), however, supports *only* \bar{S}_1 SS's because the lower Q_1 band does not contain a basis function for the \bar{S}_2 irreducible representation. Similarly, the Q_2 gap between L_2 and L_3 can only contain a \bar{S}_4 SS. In contrast to Kleinman, we, therefore, expect in the relevant energy range from -1 eV to E_F a pair of exchange-split \bar{S}_1 SS's in the Q_1 band gap and of \bar{S}_4 SS's between L_2 and L_3 . The former should exhibit an exchange splitting of approximately 300 meV, because they are purely d derived, whereas the exchange splitting of the latter should be smaller, because they are pd hybrid states. According to our analysis, no \bar{S}_2 SS's are expected below E_F .

There is another case in the literature that is subject to conflicting interpretations. This is the alleged existence of two Λ_1 SS's at $\bar{\Gamma}$ on Ni(111). Himpsel and Eastman³¹ observed an occupied, totally symmetric SS in the $L_2 - L_1$ band gap at 0.25-eV binding energy, which disperses downwards with increasing \mathbf{k}_\parallel . Passek and Donath,⁹ in a spin-resolved-inverse-photoemission study, found a partially occupied Λ_1 SS just at E_F . With increasing \mathbf{k}_\parallel it disperses upwards.

At $\bar{\Gamma}$, the symmetry analysis is of course the same as the one given above for Cu(111). Consequently *only one* $\bar{\Gamma}_1$ SS is expected. It belongs to the $L_2 - L_1$ band gap. The L_3 point produces no $\bar{\Gamma}_1$ basis functions. There is, however, an important difference to the Cu case, as was already pointed out by Himpsel and Eastman.³¹ The L_2 and the L_3 point appear in the reverse order. Therefore, the Q_2 bands terminating in the L_2 and the L_3 point, respectively, form a hybridization gap close to $\bar{\Gamma}$. This hybridization gap can support a SS. Consequently, we conclude that only one SS close to E_F exists at $\bar{\Gamma}$. It has pure p_z ($\bar{\Gamma}_1$) character. At finite \mathbf{k}_\parallel it separates into two

branches, one dispersing upwards close to the lower gap edge of the projected bulk band gap above E_F (Ref. 9) and retaining nearly pure p character. A second branch emerges away from $\bar{\Gamma}$ and disperses downwards close to the Q_2 band, which connects the L_2 and the W_3 point. For finite \mathbf{k}_{\parallel} , the lower branch is dominated by d character. In agreement with the present discussion, a numerical calculation by Borstel *et al.*³² yields also only one SS at $\bar{\Gamma}$, which splits into two components for finite \mathbf{k}_{\parallel} . The symmetry analysis provides the theoretical explanation for this behavior.

The apparent small energy difference at $\bar{\Gamma}$ between the photoemission³¹ and the inverse photoemission⁹ results could be due to a slight misalignment of the sample or to a small residual contamination [a few percent of hydrogen would be sufficient, for instance, because H is known to cause large downshifts of SS's (Ref. 33)].

In summary, projection-operator techniques can be used to obtain a symmetry analysis of SS's to generate symmetry-adapted SS wave functions, and to derive selection rules. We have used this approach to construct LCAO representations of the SS on the (111) and (110) surfaces of Cu and Ni. The SS's observed at the \bar{S} point of Ni(110) were reassigned on the basis of these symmetry considerations and the nature of the two different SS's near E_F at Ni(111) is clarified.

The author would like to thank M. Donath, P. Sandl, N. Memmel, and J. Noffke for fruitful discussions. Critical reading of the manuscript by M. Donath, N. Memmel, F. Passek, and P. Sandl as well as continuous support by V. Dose are gratefully acknowledged. The work was financially supported in part by the Deutsche Forschungsgemeinschaft through SFB 338.

-
- ¹S. D. Kevan and W. Eberhardt, in *Angle-Resolved Photoemission, Studies in Surface Science and Catalysis*, edited by S. D. Kevan (Elsevier, Amsterdam, 1992), Vol. 74.
- ²J. W. Chung, K. S. Shin, D. H. Baek, C. Y. Kim, H. W. Kim, S. K. Lee, C. Y. Park, S. C. Hong, T. Kinoshita, M. Watanabe, A. Kakizaki, and T. Ishii, *Phys. Rev. Lett.* **69**, 2228 (1992).
- ³K. E. Smith and S. D. Kevan, *Phys. Rev. Lett.* **64**, 567 (1990).
- ⁴K. H. Lau and W. Kohn, *Surf. Sci.* **75**, 69 (1978).
- ⁵U. Bischler and E. Bertel, *Phys. Rev. Lett.* **71**, 2296 (1993).
- ⁶M. F. Crommie, C. P. Lutz, and D. M. Eigler, *Nature* **363**, 524 (1993); *Science* **262**, 218 (1993).
- ⁷L. E. Urbach, K. L. Percival, J. M. Hicks, E. W. Plummer, and H. L. Dai, *Phys. Rev. B* **45**, 3769 (1992).
- ⁸W. E. Eberhardt, E. W. Plummer, K. Horn, and J. Erskine, *Phys. Rev. Lett.* **45**, 273 (1980).
- ⁹M. Donath, F. Passek, and V. Dose, *Phys. Rev. Lett.* **70**, 2802 (1993); F. Passek and M. Donath, *ibid.* **71**, 2122 (1993).
- ¹⁰J. E. Ortega and F. J. Himpsel, *Phys. Rev. Lett.* **69**, 844 (1992); J. E. Ortega, F. J. Himpsel, G. J. Mankey, and R. F. Willis, *Phys. Rev. B* **47**, 1540 (1993).
- ¹¹K. Garrison, Y. Chang, and P. D. Johnson, *Phys. Rev. Lett.* **71**, 2801 (1993).
- ¹²C. Carbone, E. Vescovo, O. Rader, W. Gudat, and W. Eberhardt, *Phys. Rev. Lett.* **71**, 2805 (1993).
- ¹³P. M. Echenique and J. B. Pendry, *Prog. Surf. Sci.* **32**, 111 (1990).
- ¹⁴S. G. Davison and M. Stęślicka, *Basic Theory of Surface States: Monographs in the Physics and Chemistry of Materials* Vol. 46 (Clarendon, Oxford, 1992).
- ¹⁵J. F. Cornwell, *Group Theory and Electronic Energy Bands in Solids* (North-Holland, Amsterdam, 1969).
- ¹⁶S. G. Louie, P. Thiry, R. Pinchaux, Y. Pétrouff, D. Chandesris, and J. Lecante, *Phys. Rev. Lett.* **44**, 549 (1980).
- ¹⁷A. Zangwill, *Physics at Surfaces* (Cambridge University Press, Cambridge, England, 1988).
- ¹⁸S. D. Kevan and R. H. Gaylord, *Phys. Rev. B* **36**, 5809 (1987).
- ¹⁹S. D. Kevan, *Phys. Rev. Lett.* **50**, 526 (1983).
- ²⁰N. V. Smith, *Phys. Rev. B* **32**, 3549 (1985).
- ²¹In most cases the irreducible representations \mathfrak{R}_m are one dimensional. If two-dimensional representations occur, it is sufficient to use the character projection operators for the symmetry classification of SS's. Only if the detailed orbital representation is looked for, does one need the diagonal elements of the transfer projection operators.
- ²²Traditionally, these SS's were classified as Λ_1 SS's, because in this particular case the Λ (ΓL) line has the same symmetry as the group of \mathbf{k}_F , namely, C_{3v} . In general, there exists no such correspondence. Hence, we label the irreducible representations with the corresponding points of the surface Brillouin zone.
- ²³P. Heimann, J. Hermann, H. Miosqa, and H. Neddermeyer, *Surf. Sci.* **85**, 263 (1979).
- ²⁴S. D. Kevan, *Phys. Rev. B* **28**, 4822 (1983).
- ²⁵P. Sandl, U. Bischler, and E. Bertel, *Surf. Sci.* **291**, 29 (1993); P. Sandl and E. Bertel, *Surf. Sci. Lett.* **302**, L325 (1994).
- ²⁶W. Jacob, V. Dose, U. Kolac, Th. Fauster, and A. Goldmann, *Z. Phys. B* **63**, 459 (1986).
- ²⁷J. Redinger, P. Weinberger, H. Erschbaumer, R. Podloucky, C. L. Fu, and A. J. Freeman, *Phys. Rev. B* **44**, 8288 (1991).
- ²⁸K.-M. Ho, B. N. Harmon, and S. H. Liu, *Phys. Rev. Lett.* **44**, 1531 (1980).
- ²⁹W. Altmann, V. Dose, and A. Goldmann, *Z. Phys. B* **65**, 171 (1986).
- ³⁰L. Kleinman, *Phys. Rev. B* **23**, 6805 (1981).
- ³¹F. J. Himpsel and D. E. Eastman, *Phys. Rev. Lett.* **41**, 507 (1978).
- ³²G. Borstel, G. Thörner, M. Donath, V. Dose, and A. Goldmann, *Solid State Commun.* **55**, 469 (1985).
- ³³G. Rangelov, N. Memmel, E. Bertel, and V. Dose, *Surf. Sci.* **236**, 250 (1990).
- ³⁴H. Eckardt and L. Fritsche, *J. Phys. F* **17**, 925 (1987).

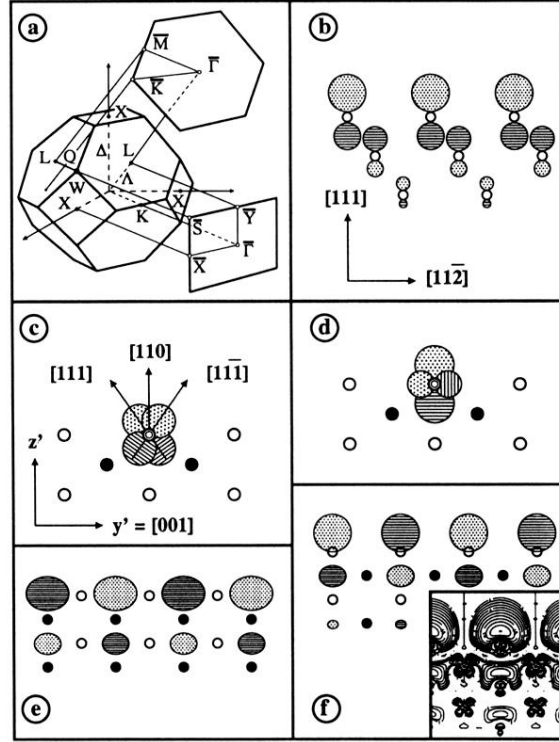


FIG. 1. (a) The fcc bulk Brillouin zone and the surface Brillouin zones for the (111) and the (110) surfaces. (b) Schematic LCAO representation of the $\bar{\Gamma}_1$ surface state on Cu(111). The open circles indicate atom positions in the three topmost Cu layers, the shaded circles represent the p_z -type orbitals. A different sign of the wave function is indicated by different shading. (c) $p_{(111)}$ orbitals of a surface atom on Cu(110). The open and closed circles represent atoms in and below the cross-section plane, respectively. (d) Symmetrized linear combinations of the $p_{(111)}$ orbitals shown in (c). (e) Schematic LCAO representation of the p_y (\bar{Y}_4) surface state at \bar{Y} on Cu(110). (f) Schematic LCAO representation of the p_z (\bar{Y}_1) surface state at \bar{Y} on Cu(110). Inset: Charge-density distribution of the Cu(110) p_z surface state after Ref. 27. Here, the cut is oriented in the $[11\bar{2}]$ azimuth.